Asian Journal of Chemistry; Vol. 35, No. 4 (2023), 1019-1024

ASIAN JOURNAL OF CHEMISTRY

https://doi.org/10.14233/ajchem.2023.27019

Structural and Luminescence Analysis of Low Temperature Solution Combustion Derived White Light Emitting $Y_{2(1-x)}Dy_{2x}Zr_2O_7$ Nanophosphors for WLEDs

SONIKA SINGH*, ANNU DALAL, MAHESH KUMAR and DEEPIKA DHATERWAL

Department of Chemistry, Chaudhary Bansi Lal University, Bhiwani-127021, India

*Corresponding author: E-mail: sonikasinghdhanger@cblu.ac.in

Received: 3 December 2022; *Accepted*: 15 March 2023; *Published online*: 30 March 2023; AJC-21204

White light emitting dysprosium doped rare-earth zirconate $Y_{2(1-x)}Dy_{2x}Zr_2O_7$ (x = 0.5 to 5 mol%) crystalline phosphors in nano-regime were obtained using urea supported solution combustion methodology at low temperature 650 ºC. Presence of fluorite structure having cubic symmetry with *Fm3m* space group was analyzed by powder X-ray diffraction patterns. Spherical shaped nanoparticles with clear boundaries were observed by surface morphological studies. Diverse elements Y, Zr, Dy and O were present in the optimized nanophosphors as examined by energy dispersive X-ray analysis. Upon near ultraviolet (NUV) excitation at 354 nm wavelength, the $Y_{2(1-x)}Dy_{2x}Zr_2O_7$ phosphors displayed the characteristic white light emanation resulted from blue and yellow emission owing to $^4F_{9/2} \rightarrow {}^6H_{15/2}$ (450-525 nm) and $^4F_{9/2} \rightarrow {}^6H_{13/2}$ (525-650) transitions, respectively. With the doping of 1.5 mol% amount of Dy^{3+} ions in $Y_{2(1-x)}Dy_{2x}Zr_2O_7$ powders showed maximum photoluminescence emission, above which intensity was quenched due to dipole-dipole interactions. In addition, $Y_{1.97}Dy_{0.03}Zr_2O_7$ nanopowders exhibit CIE colour coordinates (0.2605, 0.3145) residing in white region. The closeness of this value to the white emission coordinates of the National Television System Committee (NTSC) endorsed $Y_{2(1-x)}Dy_{2x}Zr_2O_7$ nanophosphors as fascinating candidate for displays and white light emitting diodes.

Keywords: Solution combustion, Crystallinity, White light, Luminescence.

INTRODUCTION

Advancement of illumination profoundly overcome the restrictions of limited natural light source and lead the immense growth in human civilization in past few years. Worldwide trending innovations are based on the improvement of energy saving technologies as humanity is more worried than ever before about environmental security and resource conservations. In past few years, fourth-generation solid-state illumination sources, white light emitting diodes (WLEDs) became the most energy efficient and speedily growing lighting technologies, with the potential to fundamentally revolutionize the lighting in the future [1-3]. Owing to distinguishing features such as eco-friendliness, prolonged life, low power consumption, excellent luminous, high reliability, good fidelity, long life-span and prompt response, white-LEDs have now gained a prominent position in the illumination industry. As a result, they are widely used in a variety of illuminating applications, such as panel manufacturing, solar panels, entertainment world, advertising, branding, timer knobs, vehicular illuminating, telecommunication, scanning, horticultural, forensic inks, projectors, bar-coding, food storage, kitchen equipment, civic and ambient illumination, *etc*. For the aforementioned reasons, W-LEDs have acquired a prominent stance in scientific investigations in recent years. White-LEDs are often made by integrating red, green and blue monochromatic luminescent materials in a certain way or activating yellow luminescent material with near UV lights. Regrettably, the asymmetry of brightness and higher reabsorption constitute a stumbling block to their monetization. As a result, it drives material researchers to checkout some innovative, environmentally friendly and cost-effective promising pure-phased nanophosphors [4-11].

Rare-earth zirconate compounds, $Y_2Zr_2O_7$ are pretty interesting host matrices for the lanthanide ions owing to their excellent optical, thermal, physical, mechanical characteristics and numerous uses in illumination, display field, finger printing, thermal barrier coating, photocatalysis, *etc.* [12-24]. The easy assimilation of various proportions of Ln^{3+} dopants ions as

well as codopants into the large unit cell of $Y_2Zr_2O_7$ owing to similarity in ionic sizes and valency of $Y^{3+}$and doped Ln^{3+} ions makes this lattice to act as an excellent host with dazzling luminescent properties. In past few years, numerous synthesis techniques such as solid state, hydrothermal, coprecipitation, sol-gel, vacuum sintering, *etc.* have been adopted for the synthesis of Ln^{3+} (Gd^{3+}, Er^{3+}, Eu^{3+}, Sm^{3+}, Dy^{3+}, Ho^{3+}, Tb^{3+}) doped $Y_2Zr_2O_7$ compounds [25-35]. As far as the literature studies related to doping of Dy^{3+} ions in $Y_2Zr_2O_7$ host, the urea supported solution combustion synthesis of $Y_{2(1-x)}Dy_{2x}Zr_2O_7$ nanophosphors at 650 ºC does not prevail up to now. Two studies related to codoping of Eu^{3+}/Dy^{3+} and Dy^{3+}/Li^{+} in $Y_2Zr_2O_7$ are reported by using complex sol-gel process at relatively higher temperature [36,37]. In the current work, trivalent dysprosium white light emanating $Y_{2(1-x)}Dy_{2x}Zr_2O_7$ have been effectually developed using a single step propitious and robust solution combustion synthesis at low-temperature. In this quest, Dy^{3+} ion has been selected to fabricate the desired $Y_{2(1-x)}Dy_{2x}Zr_2O_7$ nanophosphors as emission bands resided in blue range ($^4F_{9/2} \rightarrow {}^6H_{15/2}$) and yellow range($^4F_{9/2} \rightarrow {}^6H_{13/2}$) of this dopant ion well accomplished the requirement of white light displays [38,39]. All the outcomes of this innovating work signified the importance of low cost synthesis of nanophosphors for advanced display purpose like white-LEDs.

EXPERIMENTAL

White light emitting $Y_{2(1-x)}Dy_{2x}Zr_2O_7$ (x = 0. 5 to 5 mol%) nanopowders were synthesized using highly pure usher nitrates of yttrium, zirconium, dysprosium *i.e.* $Y(NO_3)_3{\cdot}6H_2O$, ZrN_2O_7, $Dy(NO_3)_3{\cdot}6H_2O$ and CH_4N_2O urea (fuel) by adopting solution combustion methodology. The pictorial illustration of complete solution combustion methodology is presented in Fig. 1.

The uniform solution of all starting reagents was kept in a preheated muffle furnace maintained at 550 ºC. The self-reliant exothermic type reaction undergoing in furnace generated the voluminous fluffy product within few minutes. The product was further sintered at 650 ºC for 1 h to get the product of fine crystallinity, which was utilized for further studies. The whole reaction occurring inside the muffle furnace that yields $Y_{2(1-x)}Dy_{2x}Zr_2O_7$ (x = 0. 5 to 5 mol%) can be represented by chemical equation as:

$$2(1\text{-}x)Y(NO_3)_3{\cdot}6H_2O + 2xDy(NO_3)_3{\cdot}6H_2O + 2ZrN_2O_7 + 8.5NH_2CONH_2 \rightarrow Y_{2(1-x)}Dy_{2x}Zr_2O_7 + \text{gaseous products (mixture of } CO_2, H_2O \text{ and } N_2)$$

Structural analysis of the synthesized $Y_{2(1-x)}Dy_{2x}Zr_2O_7$ nanophosphors were performed by utilizing Smart lab 3kw (Rigaku) multipurpose versatile XRD system, at a scan speed of 2º/min in the 2θ ranging from 10º to 80º. Microscopic images of prepared nanopowders to study the surface morphology were obtained by field emission scanning electron microscopy (FESEM) using Jeol JSM-IT 800 and elemental identification was analyzed by the energy dispersive X-ray technique (EDAX) using AZTEC software. The photoluminescence spectra in ultraviolet-visible range were examined on Hitachi F-7000 spectrofluorimeter having Xenon lamp as an excitation source. The CIE colour coordinates of $Y_{2(1-x)}Dy_{2x}Zr_2O_7$ nanophosphors were calculated using MATLAB software.

RESULTS AND DISCUSSION

The literature reveals that $Y_2Zr_2O_7$ crystallize in two structural forms one is an ordered pyrochlore with space group *Fd3m* and other is disordered fluorite structure having space group *Fm3m*. The YZO lattice shows a gradual transition from pyrochlore to anion-deficient fluorite structure if $r(RE^{3+})/r(Zr^{4+})$ become less than 1.46. In YZO compound, there is a unique seven-fold cationic coordination, that forms a stable defective fluorite structure as $r(Y^{3+})/r(Zr^{4+}) < 1.46$. The PXRD patterns of $Y_{2(1-x)}Dy_{2x}Zr_2O_7$ nanophosphors doped with 1.5 mol% and 5 mol% amount of Dy^{3+} sintered at 650 ºC for 1 h are displayed in Fig. 2. The pattern clearly shows the formation of highly crystalline single-phased defected fluorite structure with space group *Fm3m* as characterized by its four distinct peaks (222), (400), (440) and (622). The existence of two diffraction peaks

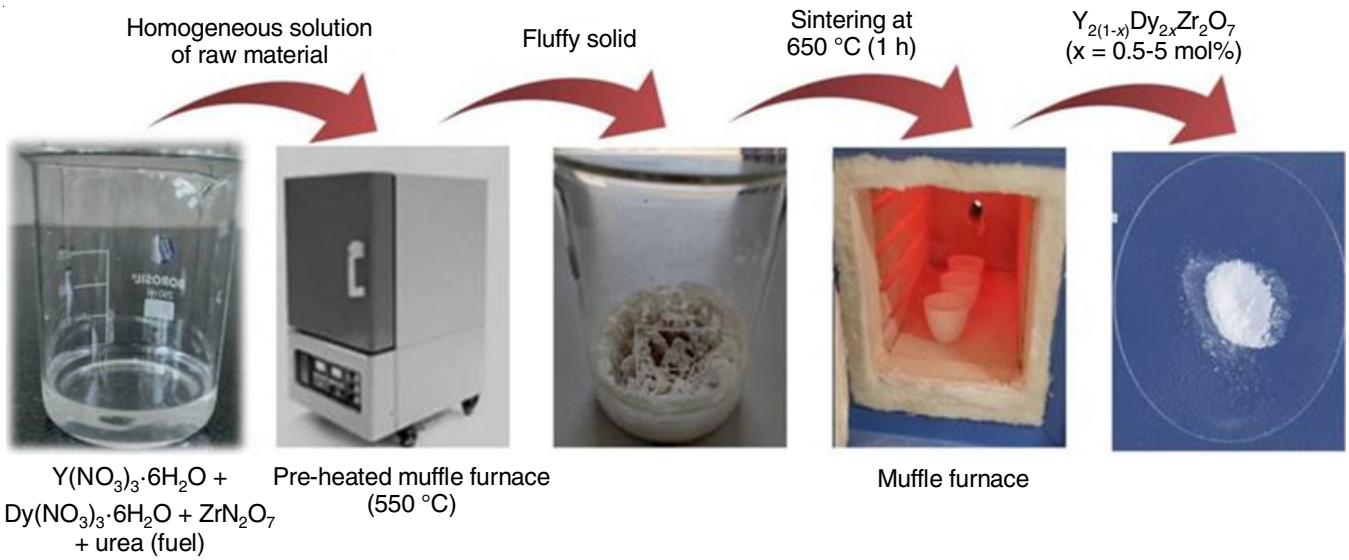

Fig. 1. Schematic illustration of solution combustion synthesis of $Y_{2(1-x)}Dy_{2x}Zr_2O_7$ (x = 0. 5 to 5 mol%) nanophosphors at 650 °C

(331) and (511) at 2θ = 36.31° and 2θ = 43.61°, respectively, indexed to the reflections of pyrochlore phase was not observed in the recorded XRD patterns. The closeness of ionic radii of Y^{3+} and Dy^{3+} lead to the successful incorporation of Dy^{3+} within the YZO host lattice as no impurity peaks were observed, although no JCPDS data corresponding to $Y_2Zr_2O_7$ phase is available yet for comparative studies [18,34]. Furthermore, a steady defective fluorite phase of $Y_2Zr_2O_7$ was retained at different mol% of Dy^{3+} suggesting that YZO can afford a large value of Dy^{3+} ions with the permissible $r(RE^{3+})/r(Zr^{4+})$ range of fluorite phase *i.e.* < 1.46. Compared with other methods, the reaction time was relatively short and pure phase formation started at relatively low temperature *i.e.* 550 ºC by SCS, this may be due to the highly exothermic nature of urea supported combustion process. The nanocrystalline aspect of synthesized $Y_{2(1-x)}Dy_{2x}Zr_2O_7$ samples was evaluated by their average crystallite size (D), calculated as per the Scherrer's equation:

$$D = \frac{0.941\lambda}{\beta\cos\theta}$$

where λ is the wavelength of CuKα radiation (0.15406 nm), β is the full width in radians at half-maximum (FWHM) and θ is the Bragg's angle of an observed X-ray diffraction peak. Taking into account the XRD data, FWHM of the strongest observed peak at (222) was selected to compute the average crystalline size for $Y_{2(1-x)}Dy_{2x}Zr_2O_7$ powder, sintered at 650 ºC for 1 h. The size obtained owing to strongest peak (2θ = 20.68º) for 1.5 mol% Dy^{3+} ions doped $Y_{2(1-x)}Dy_{2x}Zr_2O_7$ was 20.68 nm while for 5 mol% Dy^{3+} ions contents, it came out to be 20.72 nm corresponding to peak (2θ = 20.691). The result clearly confirmed that with Dy^{3+} ions contents there is no change in XRD patterns of $Y_{2(1-x)}Dy_{2x}Zr_2O_7$ host lattice.

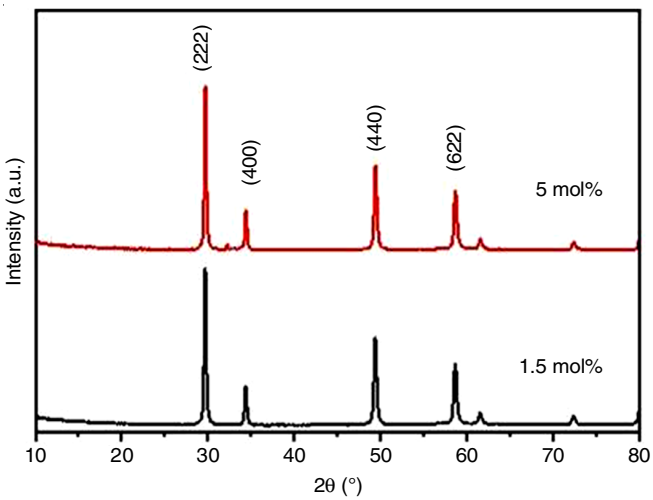

Fig. 2. Recorded PXRD patterns of $Y_{2(1-x)}Dy_{2x}Zr_2O_7$ nanophosphors doped with 1.5 mol % and 5 mol % of Dy^{3+} ions, sintered at 650°C for 1 h

The surface texture, composition and the elemental dispersion of $Y_{2(1-x)}Dy_{2x}Zr_2O_7$ (1.5 mol%) sample were investigated using FESEM and EDAX measurements. The SEM scans endorsed the uniform distribution of interconnected nearly spherical shaped particles with well-defined boundaries as depicted in Fig. 3. It is clearly seen that these crystallized particles and smooth surface morphology with some voids and porosity and these observed fissures verified the exothermic SCS of the prepared nanophosphors. The EDX spectrum and mapping analysis of $Y_{1.97}Dy_{0.03}Zr_2O_7$ powder *i.e.* YZO with 1.5 Dy^{3+} mol% has been shown in Fig. 4, which disclosed the persistence of homogeneous dispersion of all the elements *i.e.* Y, Dy, Zr and O present in $Y_{1.97}Dy_{0.03}Zr_2O_7$ powder and confirmed the effectual doping of Dy^{3+} ions in $Y_2DyZr_2O_7$ matrix at relatively low temperature in a short span by SCS (elemental peaks are depicted in Fig. 5). Thus, the above mentioned outstanding topographical traits of the prepared nanopowders enhanced their luminescence output for display field.

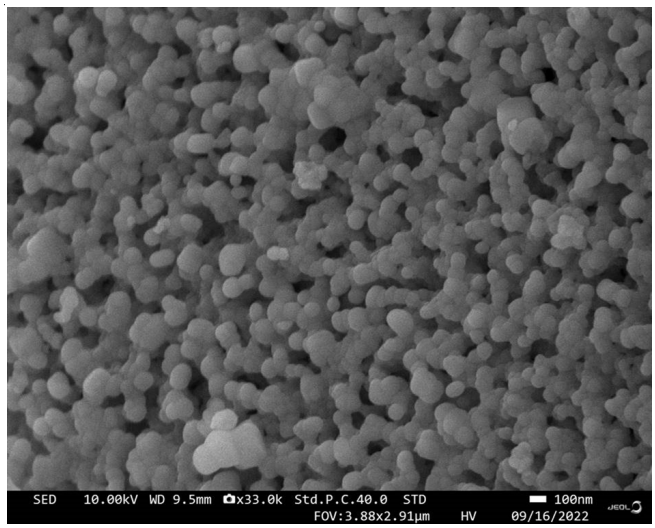

Fig. 3. SEM micrograph of $Y_{2(1-x)}Dy_{2x}Zr_2O_7$ (1.5 mol%) nanopowders sintered at 650 °C for 1 h, depicting the spherical morphology of the particles with some voids

The luminescence excitation spectrum of $Y_{2(1-x)}Dy_{2x}Zr_2O_7$ (1.5 mol%) nanophosphors was recorded at the emission wavelength (λ_{em}) of 574 nm as depicted in Fig. 6. Various sharp peaks observed in the resultant spectrum are mainly due to the 4*f*-4*f* transitions of Dy^{3+} ions in the range 300-500 nm that reside in the emission range of commercially available blue and nUV-chips of light emitting diodes. The spectrum displayed several prominent peaks at 310 nm, 329 nm, 354 nm, 389 nm, 429 nm and 470 nm attributed to the transitions $^6H_{15/2} \rightarrow {}^4K_{13/2} + {}^4H_{13/2}$, $^6H_{15/2} \rightarrow {}^6P_{3/2}$, $^6H_{15/2} \rightarrow {}^6P_{7/2}$, $^6H_{15/2} \rightarrow {}^4I_{13/2}$ $^6H_{15/2} \rightarrow {}^4G_{11/2}$ and $^6H_{15/2} \rightarrow {}^4F_{9/2}$ from ground state to the excited state, respectively. The nanocrystalline phosphors, $Y_{2(1-x)}Dy_{2x}Zr_2O_7$ (x = 0.5 to 5 mol%) were stimulated using near ultraviolet excitation wavelength (λ_{ex}) of 354 nm to record the luminescence emission spectra as shown Fig. 7. The shape and locations of the emission peaks remained same with the varying x value of Dy^{3+} ions in $Y_{2(1-x)}Dy_{2x}Zr_2O_7$ lattice, hence no distinctive traits in the emission profiles with the changing dopant concentration were identified. The emission spectra of all samples of $Y_{2(1-x)}Dy_{2x}Zr_2O_7$ revealed two prominent spikes in the blue and yellow domains at 485 and 574 nm, correspondingly, driven by the $^4F_{9/2} \rightarrow {}^6H_{15/2}$ and $^4F_{9/2} \rightarrow {}^6H_{13/2}$ transitions. It is magnetic dipole transition *i.e.* $^4F_{9/2} \rightarrow {}^6H_{15/2}$ in blue domain that is independent of the crystal field symmetry around trivalent dysprosium ions while the

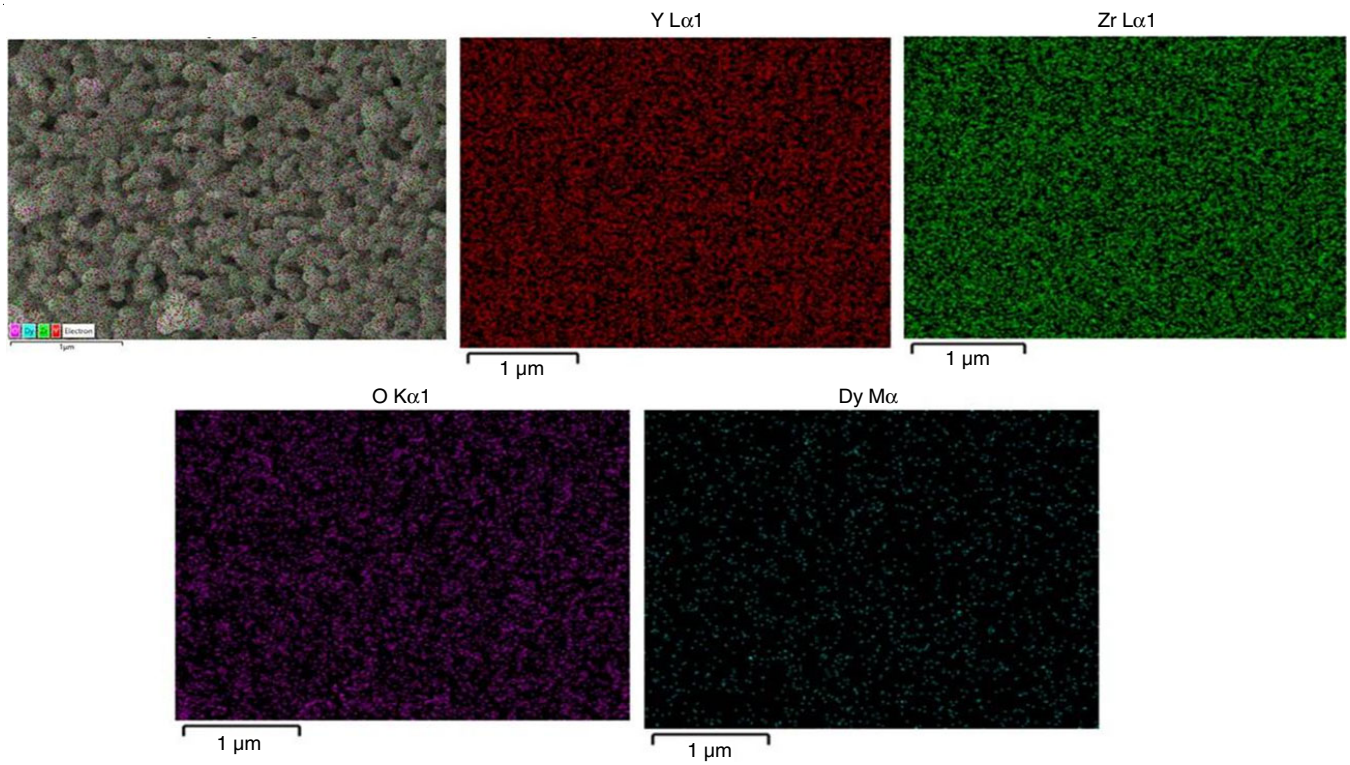

Fig. 4. EDAX spectrum showing the elemental mapping of $Y_{2(1-x)}Dy_{2x}Zr_2O_7$ (1.5 mol%) nanophosphors, sintered at 650 °C for 1 h

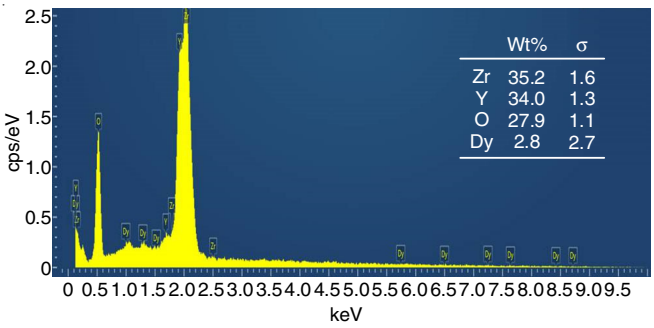

Fig. 5. EDAX spectrum of $Y_{2(1-x)}Dy_{2x}Zr_2O_7$ (1.5 mol%) showing the corresponding peaks of the constituent elements (Zr, Y, O and Dy) of the nanophosphors, synthesized by solution-combustion process

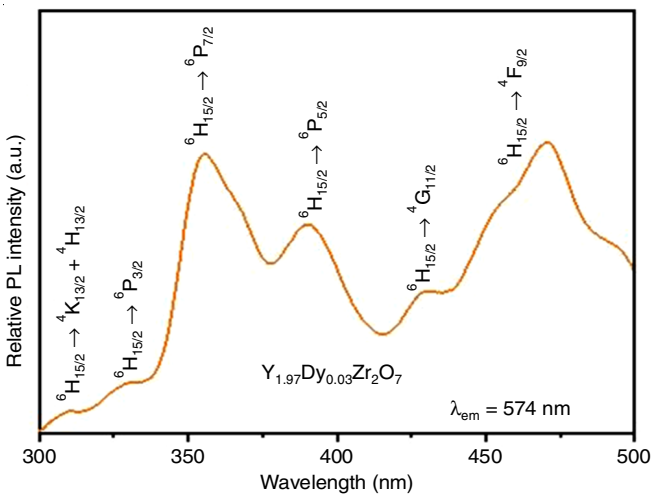

Fig. 6. Excitation spectrum of $Y_{2(1-x)}Dy_{2x}Zr_2O_7$ (1.5 mol%) nanophosphors, sintered at 650 °C for 1 h using λ_{em} of 574 nm

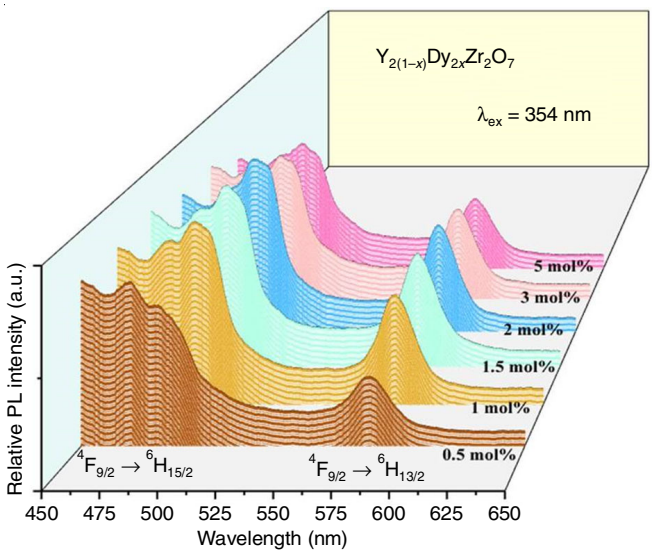

Fig. 7. Emission spectra of $Y_{2(1-x)}Dy_{2x}Zr_2O_7$ (x = 0. 5 to 5 mol%) nanophosphors, sintered at 650 °C for 1 h using λ_{ex} of 354 nm

electric dipole transition ($^4F_{9/2} \rightarrow {}^6H_{13/2}$) lying in yellow region obeys selection rule $\Delta L = 2$ and $\Delta J = 2$, get greatly influenced by the surroundings of dopant ions in the host lattice. Moreover, the presence of dopant dysprosium ions at high symmetry positions in $Y_{2(1-x)}Dy_{2x}Zr_2O_7$ lattice is justified by the dominating magnetic dipole shift associated with the magnetic dipole transition $^4F_{9/2} \rightarrow {}^6H_{15/2}$. The changes in luminous emission intensities owing to blue and yellow transitions with concentration of dysprosium ions are demonstrated in Fig. 8. It is clearly visible that the emission intensity of both transitions drops after 1.5 mol% because of concentration quenching, which takes place

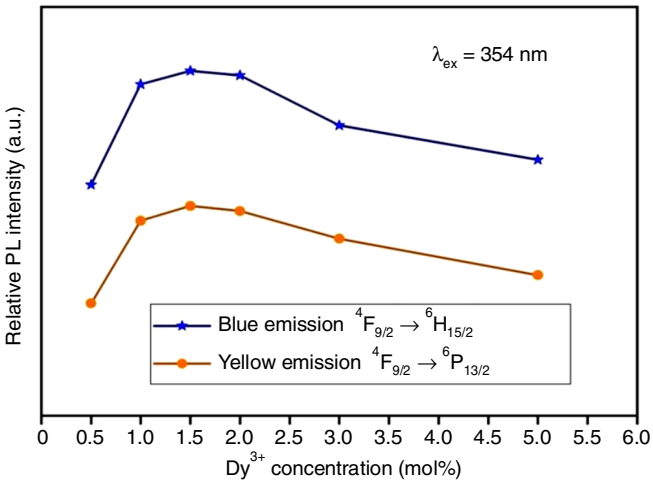

Fig. 8. Variations in photoluminescence emission intensities of the $Y_{2(1-x)}Dy_{2x}Zr_2O_7$ nanophosphors with Dy^{3+} ion concentration

as a consequence of non-radiative transfer of energy within Dy^{3+} ions, when their doping amount reached above 1.5 mol%. Using the MATLAB software, the CIE coordinates of the synthesized samples of $Y_{2(1-x)}Dy_{2x}Zr_2O_7$ for 0.5,1,1.5,2,3 and 5 mol% nanophosphors were determined as (0.236272, 0.287216), (0.253853, 0.306076), (0.260591, 0.260591), (0.256428, 0.310221), (0.256278, 0.309796) and (0.254795, 0.318181), respectively. These values have been asserted to be in the close range of NTSC colour coordinates for the white light [40-45]. A graphic investi-gation of the performance of an optimized luminous $Y_{2(1-x)}Dy_{2x}Zr_2O_7$ (1.5 mol%) phosphor using Commission International De I'Eclairage (CIE) 1931 chromaticity coordinates is well displayed in Fig. 9. The CIE illustration revealed that a careful doping of these materials could result in an effective white light generating source for displays. One crucial feature that demonstrates the readiness of phosphors for the use in WLEDs is its colour coordinates. Display devices and WLED applications could be derived from this unique attribute of producing white light from a unified system.

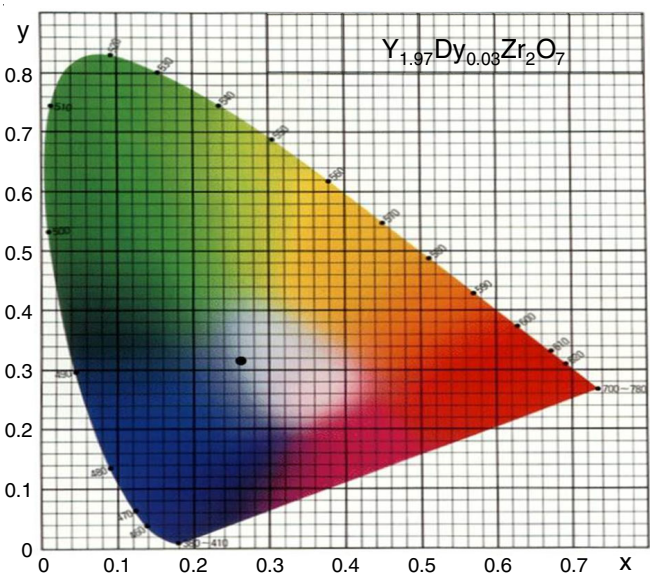

Fig. 9. CIE colour coordinate diagram of $Y_{2(1-x)}Dy_{2x}Zr_2O_7$ (1.5 mol%) nanophosphors, sintered at 650 °C for 1 h

Conclusion

A fast and extremely effective urea supported solution combustion methodology was employed to synthesize a series of Dy^{3+} doped fluorite type $Y_{2(1-x)}Dy_{2x}Zr_2O_7$ (x = 0.5 to 5 mol%) nanocrystalline phosphors, which emanate peculiar white light. An assortment of techniques, including PXRD, EDAX, SEM, PL and CIE analyses have been utilized to scrutinize the distinctive morphological and photonic traits of the synthesized nanophosphors. The PXRD of the synthesized $Y_{2(1-x)}Dy_{2x}Zr_2O_7$ nanocrystalline phosphors revealed the presence of fluorite structure with cubic symmetry and the *Fm3m* space group. The SEM image of the tailored material $Y_{2(1-x)}Dy_{2x}Zr_2O_7$ (1.5 mol%) revealed the spherical morphology of the nanophosphors. By using EDAX spectra and mapping of nanophosphors, the existence of Y, Dy, Zr and O elements in the synthesized sample was demonstrated. The stunning white emission was seen due to the flawless alignment of the blue and yellow bands. The optimized amount of trivalent dysprosium ions was found to be 1.5 mol%, after this concentration quenching phenomenon happened. It was observed that $Y_{1.97}Dy_{0.03}Zr_2O_7$ nanopowder samples CIE coordinates (0.2605, 0.3145) evenly resembled the NTSC coordinates for white emission. This validated the synthesized Dy^{3+} doped $Y_2Zr_2O_7$ nanocrystalline phosphors emission of white light and significantly helped in expanding its applications in pure phase phosphor converted WLEDs.

ACKNOWLEDGEMENTS

This work was supported by Chaudhary Bansi Lal University, Bhiwani, India vide Grant No. CBLU/DAA/2022/2136.

CONFLICT OF INTEREST

The authors declare that there is no conflict of interests regarding the publication of this article.

REFERENCES

1. Q. Guo, X. Ma, L. Liao, H. Liu, D. Yang, N. Liu and L. Mei, *J. Solid State Chem.*, **280**, 121009 (2019); https://doi.org/10.1016/j.jssc.2019.121009
2. A.K. Bedyal, D.D. Ramteke, V. Kumar and H.C. Swart, *J. Mater. Sci. Mater. Electron.*, **30**, 11714 (2019); https://doi.org/10.1007/s10854-019-01533-4
3. Y. Wang, F. Hong, L. Yu, H. Xu, G. Liu, X. Dong, W. Yu and J. Wang, *J. Lumin.*, **221**, 117072 (2020); https://doi.org/10.1016/j.jlumin.2020.117072
4. P. Sehrawat, A. Khatkar, P. Boora, M. Kumar, R.K. Malik, S.P. Khatkar and V.B. Taxak, *Chem. Phys. Lett.*, **758**, 137937 (2020); https://doi.org/10.1016/j.cplett.2020.137937
5. P. Sehrawat, R.K. Malik, P. Boora, M. Punia, M. Sheoran, P. Chhillar, S.P. Khatkar and V.B. Taxak, *Chem. Phys. Lett.*, **763**, 138243 (2021); https://doi.org/10.1016/j.cplett.2020.138243
6. J. Zhong, D. Chen, Y. Zhou, Z. Wan, M. Ding, W. Bai and Z. Ji, *Dalton Trans.*, **45**, 4762 (2016); https://doi.org/10.1039/C5DT04909A
7. A. Mancuso and G. Iervolino, *Catalysts*, **12**, 1074 (2022); https://doi.org/10.3390/catal12101074
8. E. Matioli, S. Brinkley, K.M. Kelchner, Y.L. Hu, S. Nakamura, S. DenBaars, J. Speck and C. Weisbuch, *Light Sci. Appl.*, **1**, e22 (2012); https://doi.org/10.1038/lsa.2012.22
9. J. McKittrick and L.E. Shea-Rohwer, *J. Am. Ceram. Soc.*, **97**, 1327 (2014); https://doi.org/10.1111/jace.12943

10. P. Sehrawat, A. Khatkar, P. Boora, M. Kumar, R.K. Malik, S.P. Khatkar and V.B. Taxak, *Ceram. Int*., **46**, 16274 (2020); https://doi.org/10.1016/j.ceramint.2020.03.184
11. Q. Guo, L. Liao, M.S. Molokeev, L. Mei and H. Liu, *Mater. Res. Bull*., **72**, 245 (2015); https://doi.org/10.1016/j.materresbull.2015.07.029
12. V. Sharma, S. Choudhary, P. Mankotia, A. Kumari, K. Sharma, R. Sehgal and V. Kumar, *TrAC Trends Anal. Chem*., **143**, 116378 (2021); https://doi.org/10.1016/j.trac.2021.116378
13. G. Karthick, A. Karati and B.S. Murty, *J. Alloys Compd*., **837**, 155491 (2020); https://doi.org/10.1016/j.jallcom.2020.155491
14. M. Jovaní, A. Sanz, H. Beltrán-Mir and E. Cordoncillo, *Dyes Pigments*, **133**, 33 (2016); https://doi.org/10.1016/j.dyepig.2016.05.042
15. K. Lu, Z. Liu, Y. Wang, W. Yang, H. Peng, Y. Ye, Y. Shi, J. Qi and T. Lu, *J. Alloys Compd*., **905**, 164133 (2022); https://doi.org/10.1016/j.jallcom.2022.164133
16. Y. Tong, X. Chen, Q. Wang and H. Huo, *Mater. Lett*., **157**, 106 (2015); https://doi.org/10.1016/j.matlet.2015.05.089
17. C. Kaliyaperumal, A. Sankarakumar and T. Paramasivam, *J. Alloys Compd*., **831**, 154782 (2020); https://doi.org/10.1016/j.jallcom.2020.154782
18. Y. Tong, P. Xue, F. Jian, L. Lu, X. Wang and X. Yang, *Mater. Sci. Eng. B*., **150**, 194 (2008); https://doi.org/10.1016/j.mseb.2008.04.009
19. H. Li, Q. Tao, N. Li, R. Tang, Y. Zhao, H. Zhu, P. Zhu and X. Wang, *J. Alloys Compd.*, **660**, 446 (2016); https://doi.org/10.1016/j.jallcom.2015.11.137
20. M. Saif, *J. Lumin*., **135**, 187 (2013); https://doi.org/10.1016/j.jlumin.2012.10.022
21. H. Teymourinia, Advanced Rare Earth-Based Ceramic Nanomaterials, Elsevier, pp.77-103 (2022); https://doi.org/10.1016/B978-0-323-89957-4.00004-9
22. A. Zhang, M. Lü, Z. Yang, G. Zhou and Y. Zhou, *Solid State Sci*., **10**, 74 (2008); https://doi.org/10.1016/j.solidstatesciences.2007.07.037
23. R.S. Rejith, J.K. Thomas and S. Solomon, *Solid State Ion*., **323**, 112 (2018); https://doi.org/10.1016/j.ssi.2018.05.025
24. M. Jovaní, M. Fortuño-Morte, H. Beltrán-Mir and E. Cordoncillo, *J. Eur. Ceram. Soc*., **38**, 2210 (2018); https://doi.org/10.1016/j.jeurceramsoc.2017.12.005
25. Y. Ye, Z. Tang, Z. Ji, H. Xiao, Y. Liu, Y. Qin, L. Liang, J. Qi and T. Lu, *Opt. Mater.*, **121**, 111643 (2021); https://doi.org/10.1016/j.optmat.2021.111643
26. J. Wang, K. Lu, Y. Ye, Y. Qin, W. Han and J. Qi, *Ceram. Int*., **48**, 35050 (2022); https://doi.org/10.1016/j.ceramint.2022.08.094
27. Z. Tang, Z. Huang, W. Han, J. Qi, N. Ma, Y. Zhang and T. Lu, *Scr. Mater*., **178**, 90 (2020); https://doi.org/10.1016/j.scriptamat.2019.11.007
28. Z. Tang, J. Qi, Z. Huang, L. Liang, A. Liu, Y. Ye, Y. Zhang and T. Lu, *Ceram. Int*., **48**, 4216 (2022); https://doi.org/10.1016/j.ceramint.2021.10.213
29. A. Kumar and J. Manam, *J. Alloys Compd*., **829**, 154610 (2020); https://doi.org/10.1016/j.jallcom.2020.154610
30. Ramadhin, J.K. Saluja, R. Shrivastava and V. Dubey, *Optik*, **260**, 169082 (2022); https://doi.org/10.1016/j.ijleo.2022.169082
31. J. Papan, K. Vukovic, S.P. Ahrenkiel, D.J. Jovanovic and M.D. Dramicanin, *J. Alloys Compd*., **712**, 437 (2017); https://doi.org/10.1016/j.jallcom.2017.04.139
32. A. Zhang, M. Lü, Z. Qiu, Y. Zhou and Q. Ma, *Mater. Chem. Phys*., **109**, 105 (2008); https://doi.org/10.1016/j.matchemphys.2007.10.042
33. Y. Wang, P. Darapaneni, O. Kizilkaya and J.A. Dorman, *Inorg. Chem*., **59**, 2358 (2020); https://doi.org/10.1021/acs.inorgchem.9b03226
34. Q. Du, G. Zhou, H. Zhou and Z. Yang, *Opt. Mater*., **35**, 257 (2012); https://doi.org/10.1016/j.optmat.2012.08.014
35. A. Kumar and J. Manam, *Ceram. Int*., **48**, 13615 (2022); https://doi.org/10.1016/j.ceramint.2022.01.241
36. A. Zhang, P. Yang, Y. Cao and Y. Zhu, *Adv. Mater. Lett*., **2**, 322 (2011); https://doi.org/10.5185/amLett.2011.3042am2011
37. Q. Du, G. Zhou, J. Zhou, X. Jia and H. Zhou, *J. Alloys Compd*., **552**, 152 (2013); https://doi.org/10.1016/j.jallcom.2012.10.074
38. M. Dhanalakshmi, H. Nagabhushana, G.P. Darshan, R.B. Basavaraj, and B. Daruka Prasad, *J. Sci.: Adv. Mater. Devices*, **2**, 22 (2017); https://doi.org/10.1016/j.jsamd.2017.02.004
39. P. Sehrawat, A. Khatkar, S. Devi, A. Hooda, S. Singh, R.K. Malik, S.P. Khatkar and V.B. Taxak, *Chem. Phys. Lett*., **737**, 136842 (2019); https://doi.org/10.1016/j.cplett.2019.136842
40. Sonika, S.P. Khatkar, A. Khatkar, R. Kumar and V.B. Taxak, *J. Electron. Mater*., **44**, 542 (2015); https://doi.org/10.1007/s11664-014-3465-y
41. C.M. Mehare, N.S. Dhoble, C. Ghanty and S.J. Dhoble, *J. Mol. Struct*., **1227**, 129417 (2021); https://doi.org/10.1016/j.molstruc.2020.129417
42. J. Xian, S. Yi, Y. Deng, L. Zhang, X. Hu and Y. Wang, *Physica B Condens. Matter*, **483**, 19 (2016); https://doi.org/10.1016/j.physb.2015.12.022
43. M. Sheoran, P. Sehrawat, N. Kumari, S.P. Khatkar and R.K. Malik, *Chem. Phys. Lett*., **773**, 138608 (2021); https://doi.org/10.1016/j.cplett.2021.138608
44. T. Krishnapriya, A. Jose, T. Anna Jose, C. Joseph, N.V. Unnikrishnan and P.R. Biju, *Adv. Powder Technol*., **32**, 1023 (2021); https://doi.org/10.1016/j.apt.2021.02.003
45. R. Shrivastava, J. Kaur and V. Dubey, *J. Fluoresc*., **26**, 105 (2016); https://doi.org/10.1007/s10895-015-1689-8